WDS'25 Proceedings of Contributed Papers — Physics, 84–93, 2025. ISBN 978-80-7378-532-1 © MATFYZPRESS

Full-Wave Modeling of Whistler Wave Propagation Through the Martian Ionosphere

K. Rosická, O. Santolík, and I. Kolmašová
Institute of Atmospheric Physics, Czech Academy of Science Prague, Czech Republic.
Charles University, Faculty of Mathematics and Physics, Prague, Czech Republic.

F. Němec
Charles University, Faculty of Mathematics and Physics, Prague, Czech Republic.

Abstract. Lightning flashes have been observed on several planets in the Solar System. However, atmospheric discharges have not yet been detected on Mars, despite theoretical models predicting their occurrence within dust devils. We present a full-wave simulation of an electromagnetic signal generated by a hypothetical lightning discharge. We show that it can exceptionally propagate through the Martian ionosphere in the form of a whistler, which would be detectable by spacecraft orbiting Mars. In our work, we consider ionospheric plasma with a Chapman profile consisting of electrons and O_2^+ ions under the conditions of a region with a strong crustal magnetic field. We model the transmission of a single plane wave through the ionosphere with different initial wave vector directions, wave polarization and frequencies. Under these conditions, we investigate the causes of attenuation, such as different types of collisions or reflection of the wave at the lower boundary of the ionosphere. In this work, we demonstrate that the transmition of whistler signals through the Martian ionosphere is possible, but the favorable conditions are rare.

Introduction

Since the end of the 19th century, lightning generated whistlers have been observed on the telephone lines as disruptions with a gradually decreasing frequency within the audible range [*Ratcliffe and Storey*, 1953]. With the development of the spacecraft missions, the lightning generated whistlers were observed from the orbit as waves propagating along the magnetic field lines or slightly deviating from them. Nowadays, whistlers are a standard method of lightning observation providing additional information about the properties of the ionosphere and magnetosphere. Whistlers have also been used as the evidence of existence of lightning discharges on Jupiter [*Gurnett et al.*, 1979] and Neptune [*Gurnett et al.*, 1990] and one whistler event was also detected on Saturn [*Akalin et al.*, 2006]. Detailed review of planetary lightning detection can be found in *Aplin and Fischer* [2017, 2019] or *Aplin et al.* [2020]. Additionally, whistler dispersion can be used as an indicator for the plasma density profile along the whistler's trajectory, and their amplitude can be used to estimate the energy of the lightning discharge [*Scarf et al.*, 1981]. While most propagation processes can be explained in the same way on different planets, attenuation of whistlers during their propagation through the ionosphere depends heavily on various parameters, such as the density profile, ion composition and planetary magnetic field. A full-wave model of the terrestrial ionosphere by *Graf et al.* [2013] shows, that the inclination of the local magnetic field and the direction of the wave vector are also important parameters influencing the attenuation.

The presence of atmospheric discharges in the Martian atmosphere has not yet been confirmed, despite an extensive search at high frequencies of a few MHz [*Gurnett et al.*, 2010], and at low frequencies of a few Hz coresponding to Schumann resonances [*Anderson et al.*, 2011]. Although some non-thermal radiation was detected during dust storms [*Ruf et al.*, 2009], a direct evidence of lightning or similar electric discharge phenomena remains lacking. In contrast to the absence of observational confirmation, theoretical studies of *Barth et al.* [2016] and laboratory experiments by *Krauss et al.* [2003] suggest that the charge separation within Martian dust storms could generate electric fields exceeding the local dielectric breakdown threshold [*Riousset et al.*, 2020].

In this work, we attempt to study the importance of different parameters of the whistler wave propagation through Martian ionosphere on the hypothetical signals, measured on orbiting spacecraft, such as Mars Atmosphere and Volatile Evolution (MAVEN) [*Jakosky et al.*, 2015]. On the MAVEN spacecraft, electromagnetic waves are measured by the Langmuir Probe and Waves instrument (LPW) [*Andersson et al.*, 2015] which uses a single-axis electric antenna to record data in three frequency bands, 0–500 Hz, 100–8000 Hz, and 100 Hz–1.6 MHz. In the magnetized plasma, electromagnetic waves can propagate in the whistler mode at frequencies below both the local plasma frequency and the electron cyclotron frequency, or in the free-space mode at frequencies above these limits. Since this study focuses on the whistler-mode propagation, we restrict our analysis to waves below the lower of these two characteristic frequencies. The resulting evolution of wave attenuation across this frequency range can help to predict the expected intensity variations of potential whistler signals, which could be detectable from orbit.

Full-wave method

In this work, the full-wave method introduced by *Lehtinen and Inan* [2008, 2009] was used. This method models a plane wave propagating through a horizontally stratified ionosphere by solving the Maxwell equations at each interface. This method is suitable for modeling wave propagation in the lower ionosphere with high vertical density gradients, which is the region, where ray-tracing simulations stops working due to the the Wentzel–Krammers–Brillouin (WKB) condition. It has also advantage of accounting for the wave attenuation due to refraction, but the model is valid only when horizontal gradients are negligible. In the full-wave model, four wave modes (two up going and two down going) are considered in each layer using the cold plasma approximation. The propagation of the wave in each layer is modeled using a dielectric tensor of a magnetized plasma medium

$$\epsilon = \begin{pmatrix} S & -iD & 0 \\ iD & S & 0 \\ 0 & 0 & P \end{pmatrix} \tag{1}$$

expressed by Stix coefficients [*Stix*, 1992] with collisions included. In this model, we use the wave phase convention of $e^{i(\mathbf{k}\cdot\mathbf{r}-\omega t)}$to adjust the positive imaginary part of $\mathbf{k}$ for waves absorbed in the upward direction.

Stix coefficients with collision terms

The Stix parameters were modified to account for collissions of different types of particles according to *Melnik and Parrot* [1999]. The equations of motion for particles in a cold plasma are modified by adding the collision frequencies (in s^{-1}) for momentum transfer of electrons with neutrals ν_{en}, ions with neutrals ν_{in}, electrons with ions ν_{ei} and ions with electrons ν_{ie} [*Huba and Rowland*, 1993] as:

$$\frac{\partial \mathbf{v_e}}{\partial t} = \frac{e}{m_e}\left(\mathbf{E} + \mathbf{v_e} \times \mathbf{B}\right) - \nu_{en}\mathbf{v_e} - \nu_{ei}(\mathbf{v_e} - \mathbf{v_i}) \tag{2}$$

$$\frac{\partial \mathbf{v_i}}{\partial t} = \frac{q_i}{m_i}\left(\mathbf{E} + \mathbf{v_i} \times \mathbf{B}\right) - \nu_{in}\mathbf{v_i} - \nu_{ie}(\mathbf{v_i} - \mathbf{v_e}) \tag{3}$$

This equation leads to modified Stix coefficients

$$S = 1 + \frac{i}{\omega\epsilon_0}\frac{en}{B}\frac{(\Lambda_e\Lambda_i - \Omega_e\Omega_i - \nu_{ei}\nu_{ie})\left[\Omega_i(\Lambda_e - \nu_{ei}) - \Omega_e(\Lambda_i - \nu_{ie})\right]}{(\Lambda_e^2 + \Omega_e^2)(\Lambda_i^2 + \Omega_i^2) - 2\Lambda_e\Lambda_i\nu_{ei}\nu_{ie} + 2\Omega_e\Omega_i\nu_{ei}\nu_{ie} + \nu_{ei}^2\nu_{ie}^2} \tag{4}$$

$$D = \frac{1}{\omega\epsilon_0}\frac{en}{B}\frac{\Omega_e^2\Lambda_i^2 - \Omega_i^2\Lambda_e^2 - (\Omega_e\nu_{ie} - \Omega_i\nu_{ei})(\Lambda_e\Omega_i + \Lambda_i\Omega_e)}{(\Lambda_e^2 + \Omega_e^2)(\Lambda_i^2 + \Omega_i^2) - 2\Lambda_e\Lambda_i\nu_{ei}\nu_{ie} + 2\Omega_e\Omega_i\nu_{ei}\nu_{ie} + \nu_{ei}^2\nu_{ie}^2} \tag{5}$$

$$P = 1 + \frac{i}{\omega}\frac{e^2 n}{\epsilon_0}\frac{\frac{1}{m_e}(\Lambda_i - \nu_{ie}) + \frac{1}{m_i}(\Lambda_e - \nu_{ei})}{\Lambda_e\Lambda_i - \nu_{ei}\nu_{ie}} \tag{6}$$

where Ω_e and Ω_i are the cyclotron frequencies of electrons and ions in $\mathrm{rad.s^{-1}}$ with the sign of the charge, $\Lambda_e = -i\omega + \nu_{en} + \nu_{ei}$ and $\Lambda_i = -i\omega + \nu_{in} + \nu_{ie}$ where ω is angular frequency of the wave in $\mathrm{rad \cdot s^{-1}}$, n is the local plasma density in $\mathrm{m^{-3}}$, B is the magnitude of the local magnetic field in T, e is the elementary charge in C, m_e is the mass of the electron and m_i is the mass of the ion, both in kg.

The collision frequencies for momentum transfer are the only difference between this theory and the standard theory of cold plasma. These frequencies were computed using a set of equations from *Melnik and Parrot* [1999].

$$\nu_{en} = 2.12 \cdot 10^{16}\, n_n T_e^{1/2} \tag{7}$$

$$\nu_{in} = 2.6 \cdot 10^{-15}\, n_n M^{-1/2} \tag{8}$$

$$\nu_{ei} = 3.62 \cdot 10^{-6}\, n_i T_e^{-3/2} \ln \Lambda \tag{9}$$

$$\nu_{ie} = \nu_{ei} \frac{m_e}{m_i} \tag{10}$$

where $\ln \Lambda$ is Coulomb logarithm, which can be estimated as $\Lambda = 1.23 \cdot 10^7\, T_e^{3/2} n_e^{-1/2}$ where n_e is the electron density in $\mathrm{m^{-3}}$, which is the same as the ion density n_i, n_n is the neutral density in $\mathrm{m^{-3}}$ and T_e is the electron temperature in kelvins and M is the mean molecular weight of the ions.

Parameters of the plasma medium

The simulation was performed using a different set of initial conditions, including frequency, wave vector direction, wave polarisation, ionospheric parameters and intrinsic magnetic field. The Chapman profile was used as a plasma density profile

$$n(z) = n_m \exp\left(0.5(1 - \chi - \exp(-\chi))\right) \tag{11}$$

$$\chi = \frac{z - z_m}{H} \tag{12}$$

where $n_m = 5 \cdot 10^3\,\mathrm{cm^{-3}}$ is the density at the maximum, $z_m = 150\,\mathrm{km}$ is the height of the maximum density and $H = 30\,\mathrm{km}$ is the scale height. These parameters were used as typical nighttime ionosphere parameters at Mars. During the daytime, the ionospheric parameters are different and highly dependent on the solar zenith angle (SZA), as described in detail in *Němec et al.* [2011]. The relations are supposed to be valid for SZA lower than 75°. In general, the maximum density can reach 30 times larger values during the day, while height of maximum density is usuallyaround 125–140 km and the scale height is also lower with values around 12–15 km. These daytime parameters give us the variation limits of realistic values of ionospheric parameters used in the next chapters.

In this study, we considered the plasma to be composed of electrons and single ion species, O_2^+, which is the most abundant ion in the Martian ionosphere [*Peter et al.*, 2021]. Other common ions, such as NO^+, CO^+ have their masses very similar to that of O_2^+. In the upper ionosphere, O^+ ions can also become significant [*Peter et al.*, 2021], however, the magnetic field in this region is typically weak, so the influence of the ions on the attenuation is negligible. Overall, the frequencies of interest in this study are 2–3 orders of magnitude higher than the ion cyclotron frequencies, so the effects of the ion species can be safely neglected.

Neutral density is modeled as exponentially decreasing density of molecular oxygen O_2 and carbon dioxide CO_2

$$n_{CO_2}(z) = 2 \cdot 10^{12} \cdot \exp\left(\frac{(z - 100\,\mathrm{km})\log(0.5 \cdot 10^{-5})}{100}\right)\,\mathrm{cm^{-3}} \tag{13}$$

$$n_{O_2}(z) = 2 \cdot 10^{9} \cdot \exp\left(\frac{(z - 120\,\mathrm{km})\log(2 \cdot 10^{-3})}{180}\right)\,\mathrm{cm^{-3}} \tag{14}$$

$$n(z) = n_{CO_2}(z) + n_{O_2}(z) \tag{15}$$

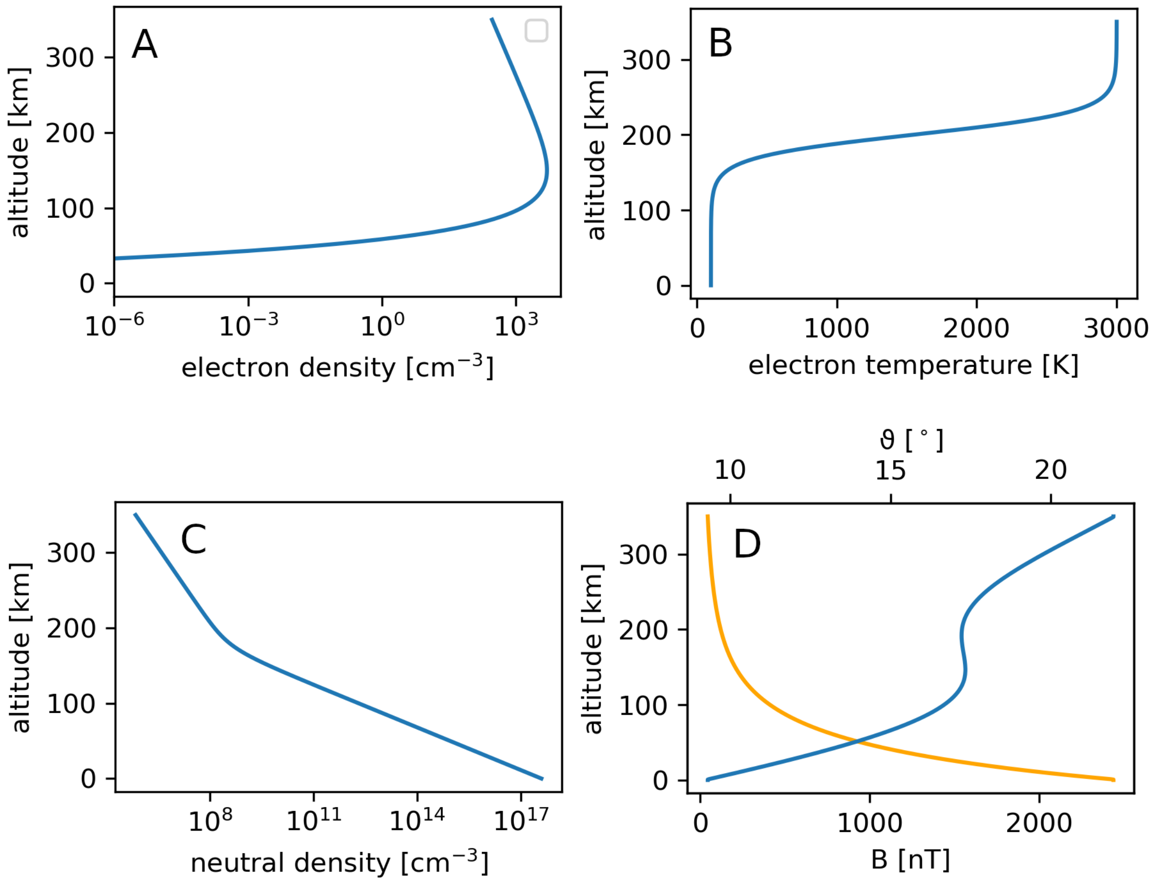

Figure 1. Parameters of the model ionosphere: A) electron density profile modeled as the Chapman profile, B) electron temperature profile, C) neutral density profile, D) the magnetic field strength and inclination from the vertical direction derived from *Gao et al.* [2021]

The last ionospheric parameter is the electron temperature, which was modeled as

$$T_e(z) = \frac{T_1 + T_2}{2} + \frac{T_2 - T_1}{2} \tanh\left(\frac{z - z_0}{H}\right) \tag{16}$$

where $T_1 = 100\,\mathrm{K}$ is the temperature at the lower boundary, $T_2 = 3000\,\mathrm{K}$ is the temperature at the upper boundary, $z_0 = 200\,\mathrm{km}$ is the altitude at which an average temperature of 1550 K is reached.

These parameters are plotted in Figure 1 along with the magnetic field profile in an area with a high intrinsic magnetic field. For the purpose of the model, we are using the magnetic field amplitude B and its inclination from the vertical direction computed as $\vartheta = \arccos\left(B_r/B\right)$, where B_r is the vertical component of the magnetic field. This profile was modeled by the spherical harmonic model of Martian magnetic field by *Gao et al.* [2021] based on Mars Global Surveyor (MGS) and MAVEN measurements of magnetic field at night under magnetically quiet conditions. We used the magnetic field profile from this model at planetographic latitude of $-73.4°$ and longitude of $-125.8°$. This location was chosen as a place with a strong nearly verticly oriented magnetic field. Planetary magnetic field at an altitude of 350 km has the same or higher amplitude than approximately 93 % of the planet.

Computed values of the collision frequencies for momentum transfer of the individual species as well as the plasma and cyclotron frequencies are shown in Figure 2. For this profile, the minimum electron cyclotron frequency is approximately 1128 Hz, so we can expect whistler to propagate at frequencies below this value. On the other hand, maximum plasma frequency is approximately 630 kHz, so electromagnetic waves at higher frequencies are expected to propagate in the free space mode with negligible attenuation. For electromagnetic waves in the kHz range below the maximum plasma frequency,

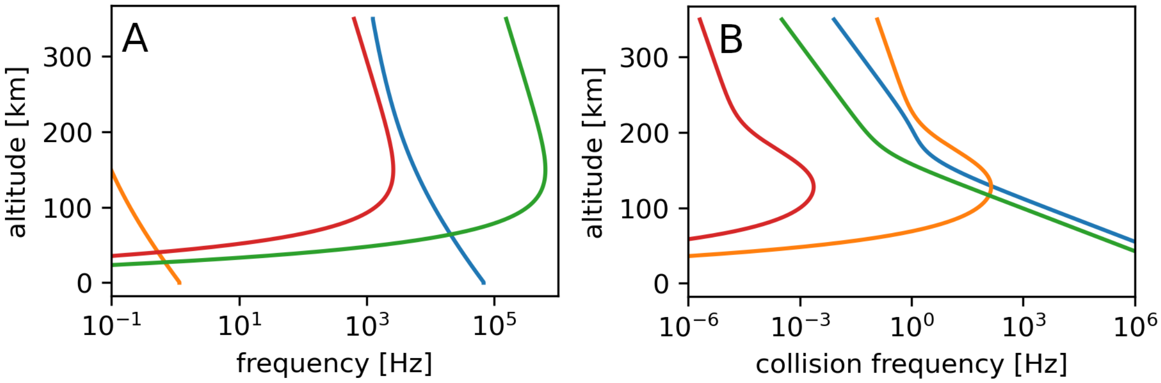

Figure 2. Altitude profiles of characteristic frequencies: A) cyclotron and plasma frequencies for electrons (blue, green) and O_2^+ ions (orange, red) at different altitudes, B) collision frequencies for momentum transfer for electron–neutral collision (blue), ion–neutral collisions (green), electron–ion collisions (orange) and ion–electron collisions (red)

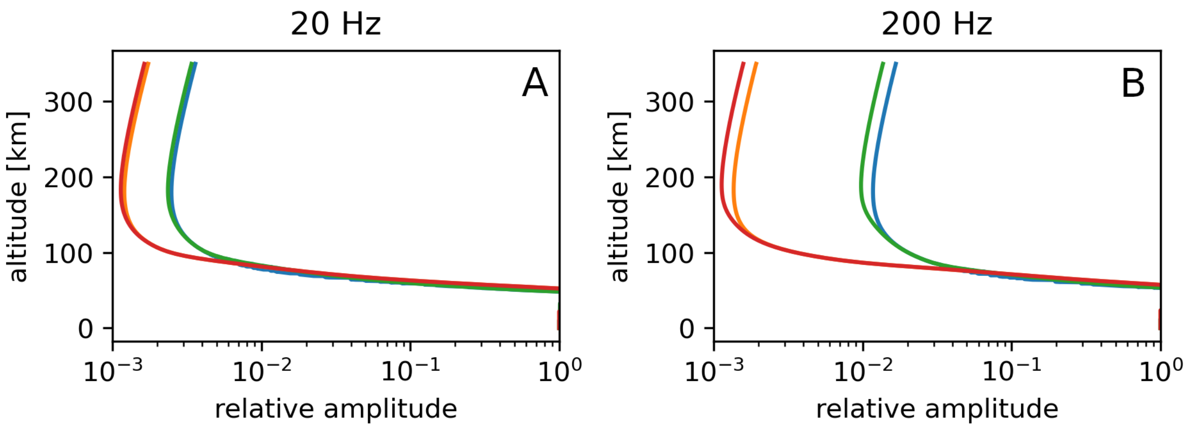

Figure 3. Relative amplitude of electric field as a function of altitude without collisions (blue), including electron–ion and ion–electron collisions (green), including only collisions with neutrals (orange) and with all type of collisions (red), A) wave frequency of 20 Hz , B) wave frequency of 200 Hz

the environment is unable to carry any wave mode, so these frequencies are completely attenuated.

Moreover, we examined the influence of the arbitrary thickness of discrete horizontally stratified layers used in our full wave numerical calculations, revealing that 1 km-thick layers give the same results as 500 m-thick layers with a relative error of 10^{-4} (for a simulation with collisions). To make the computation efficient, 1 km-thick layers were used.

Causes of attenuation

We focus on the three main sources of the attenuation: backward reflection, attenuation by collisions with neutrals and attenuation by electron–ion collisions. For this purpose, we plotted the relative amplitude of electric field versus altitude at two different frequencies including different combinations of collisions. Figure 3 shows that the attenuation is slightly lower without collisions than with both types of collisions. However, most of the attenuation still comes from refraction at the bottom of the ionosphere rather than from collisions. While collisions with neutrals are the dominant type of collisions, the contribution of electron–ion collisions is more important mainly at higher altitudes, where this type of collisions becomes dominant. An increase in the amplitude of the electric field at the uppermost part of the ionosphere can be caused by a combination of two effects. The first one is a decrease of the refractive index in the upper part of the ionosphere, which causes an increase of the ratio of the electric to the magnetic fields while conserving the Poyning flux. The second effect is an evanescent wave reaching

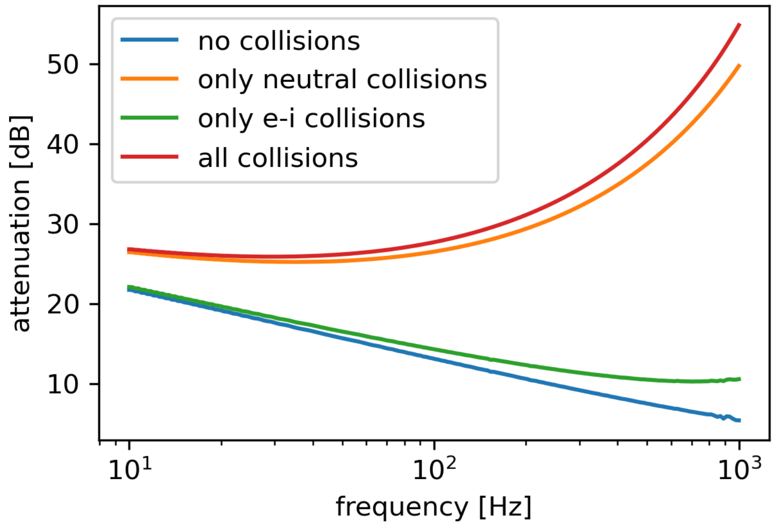

Figure 4. Attenuation of the wave after a transfer through the ionosphere according to the wave frequency without collisions (blue), including electron–ion and ion–electron collisiončs (green), including only collisions with neutrals (orange) and with all type of collisions (red)

a less dense plasma environment, where the wave vector becomes real again in a classical analogue of quantum tunneling.

By comparing plots of two different frequencies, we can see that for higher frequencies, the resulting amplitude is similar, but collisions have a much greater influence. To get a complete picture, we plotted a graph showing the resulting attenuation with including different types of collisions as a function of frequency, as shown in Figure 4. This figure shows that the attenuation due to refraction at the lower boundary decreases with frequency, while the influence of collisions increases with frequency. These two opposing effects result in attenuation that remains almost constant up to around 100 Hz, gradually increasing at higher frequencies. Therefore, we choose 20 Hz and 200 Hz as representative frequencies for refraction-dominated and collision-dominated attenuation and we use these two frequencies in the rest of the study.

Influence of wave vector direction and wave polarization

The direction of the wave vector under the ionosphere also has a significant impact on the attenuation of the waves. We tried different directions marked by the angle α from the vertical. A positive angle indicates an inclination in the same direction as the magnetic field. When changing the wave direction, wave polarization becomes important. There are two natural polarization types: left-hand polarization, which is highly attenuated (more than 100 dB attenuation) and right-hand polarization, which makes up the main part of the transmitted wave. A natural wave is a combination of these two polarizations. This is why we tried two linear combinations of the two circularly polarized waves, resulting in linearly polarized waves. We used two dominant directions called p-polarization and s-polarization. In a p-polarized wave, the electric field is parallel to the incident plane, and in an s-polarized wave, the electric field is perpendicular to the incident plane. The attenuation according to the angle α between the vertical and the wave vector direction is shown in Figure 5.

Because the resonance cone is very wide ($> 80°$) and the R wave refractive index is very high (more than 2000 at 20 Hz and around 670 at 200 Hz), the Brewster angle for the total transmission of p waves in isotropic media is larger than $89.9°$. The differences in attenuation can be then explained by refraction at the lower boundary of the ionosphere.

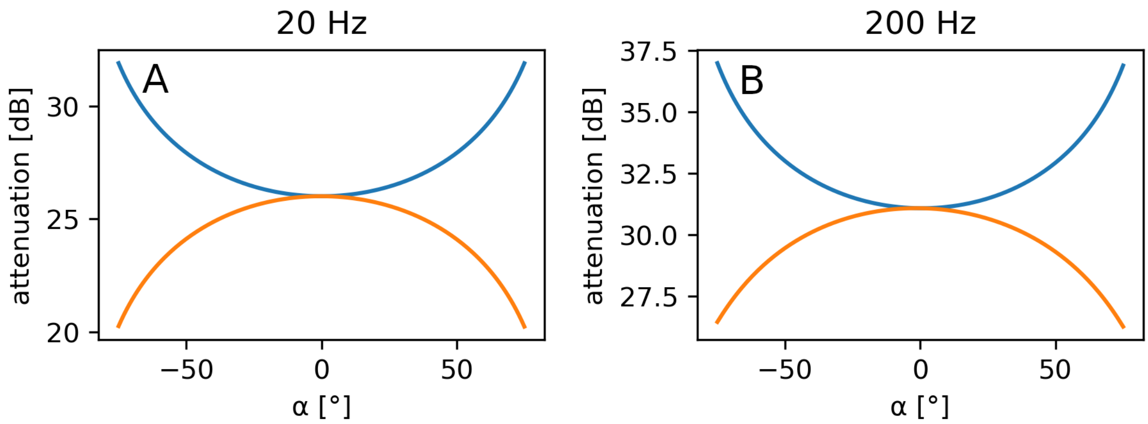

Figure 5. Attenuation of the wave for different angle α of the initial wave vector with respect to the vertical direction for s polarisation (blue) and p polarisation (orange), A) wave frequency of 20 Hz, B) wave frequency of 200 Hz

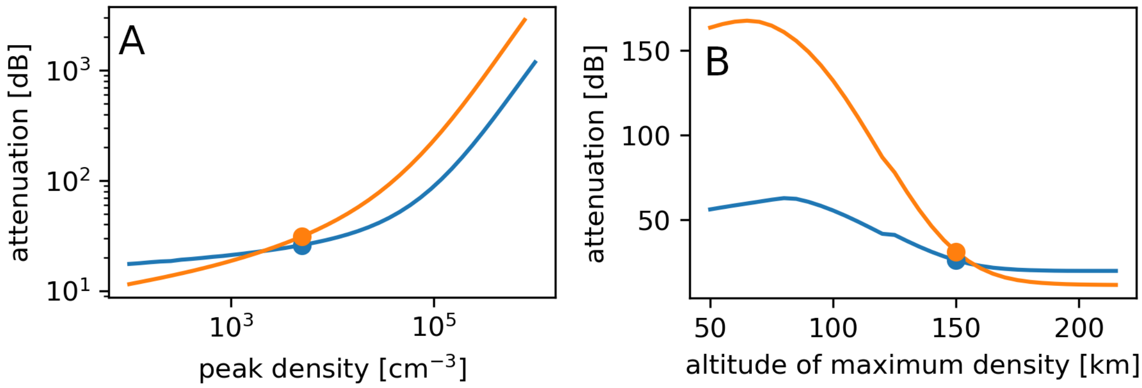

Figure 6. Attenuation of the wave for varying ionospheric parameters, the dots show the original model values for the wave frequencies of 20 Hz (blue) and 200 Hz (orange) A) maximum ionospheric density, B) altitude of the maximum ionospheric density

Influence of the ionospheric parameters

We also tried to vary ionospheric parameters. We ran simulations with changing the ionospheric peak density and changing the altitude of ionospheric maximum density, both with a constant scale height. The effects of these changes are shown in Figure 6. As the peak ionospheric density increases, attenuation of the wave increases significantly (Figure 6A), with a faster increase for the 200 Hz wave. From Figure 6, we can see that for peak densities corresponding to the daytime ionosphere (10^5 cm^{-3}), the attenuation is much higher, on the order of hundreds of dB. In this case, the ionospheric density is multiplied by a constant factor at all the altitudes (resulting from the Chapman profile), so the wave hits a region of the ionosphere with the same plasma frequency as the wave frequency at a lower altitude. To evaluate this effect, we plotted the attenuation as a function of the ionospheric peak density altitude, while conserving all the other remaining parameters. This is shown in Figure 6B. This graph shows, that at lower altitudes, the attenuation is much higher, which may be caused by higher a neutral density resulting in higher collision frequencies with neutrals at the lower boundary of the ionosphere, where most of the attenuation occurs. This effect is more significant for waves with a higher frequency, because these waves are more affected by collisions. For higher altitudes, the attenuation remains nearly constant after a threshold altitude, with lower attenuation for higher frequencies, which is consistent with the decreasing effect of collisions. This effect also supports higher attenuation during the daytime, when the z_m value is lower.

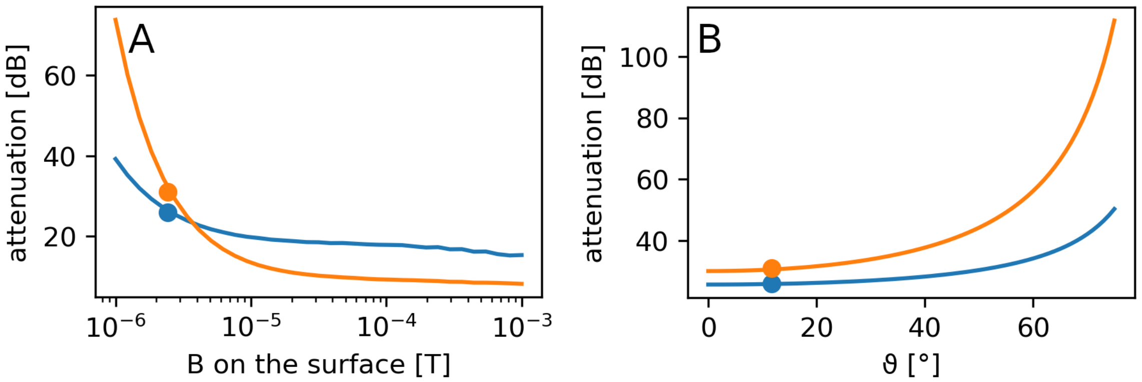

Figure 7. Attenuation of the wave under varying magnetic field, the dots show the original model values for the waves frequencies of 20 Hz (blue) and 200 Hz (orange), A) surface amplitude of the magnetic field with the same dipole position B) the angle ϑ between the magnetic field and vertical direction

Influence of the intrinsic magnetic field

The second important environmental factor is the intrinsic magnetic field. To evaluate its influence, we locally fitted the original global field model with a dipole, achieving a very good fit with a dipole center located 120 km below the surface. Perfoming this fit over the whole surface on a $2° \times 2°$ grid, we can see that a typical dipole depth is shallower with a mean value around 100 km. Note that, that for locations with shallower dipole centre, the magnetic field decreases faster and the attenuation is larger. Using the same depth, but changing the magnetic momentum we observed a decrease in attenuation as the magnetic field increases, as shown in Figure 7A. This plot shows that for both analyzed frequencies, there is a rapid decrease of attenuation at low magnetic fields, followed by a plateau region with nearly constant attenuation and then another decrease at very high fields. However, we must consider that the original magnetic field is one of the strongest occurring on Mars so the attenuation will be much higher in most locations on Mars.

Figure 7B shows the dependence of attenuation on the inclination of the magnetic field from the vertical direction. For this simulation, a constant inclination was used for all altitudes and original magnitude of the magnetic field. We can see, for low angles between the vertical and magnetic field, the dependence is very weak, but for higher inclinations over 50 °, the attenuation increases very quickly.

Discussion of plausible scenarios

In this study, we performed a detailed analysis of the attenuation for a specific location characterized by a strong vertical magnetic field in the nightside ionosphere. Extending this approach to the whole planet using the $2° \times 2°$ grid, we found that the magnetic field in this location is stronger than for 93 % of the planet.

Estimating the likehood of whistler detection by spacecraft is challenging, primarily due to the unknown amplitude of the source signal. However, assuming the signals are relatively weak, we consider an attenuation of 50 dB (five orders of magnitude) as the upper limit for their detectability. During nighttime, for the 20 Hz signal, the attenuation is 50 dB or less for 13.5 % of the surface, while for 200 Hz, this fraction decreases to 4.9 %.

Under daytime ionospheric conditions with SZA$= 75°$, these values decrease to 1.4 % for 20 Hz and 0.3 % for 200 Hz wave. For SZA$= 0°$, (which occurs only at low latitudes near the equator) the area of regions permitting transmission with an attenuation below 50 dB decrease even further, to 0.3 % for 20 Hz wave and only 0.02 % for 200 Hz wave. The results are summarized in Table 1. Based on these results, we conclude that the detection of lightning-generated whistler waves on Mars is possible, but highly improbable, particularly on the dayside of the planet.

Table 1. Percentage of the planet surface with the attenuation lower than 50 dB under specified conditions for 20 Hz and 200 Hz signal computed on $2° \times 2°$ grid

type of ionosphere	20 Hz	200 Hz
night time	13.5 %	4.9 %
day, SZA= 75°	1.4 %	0.3 %
day, SZA= 0°	0.3 %	0.02 %

Conclusion

In this study, we presented a full-wave model of wave propagation through the ionosphere, taking into account collisions in the plasma, and applied this model to the Martian ionosphere. We examined the influence of various wave properties, such as frequency, wave vector direction and wave polarization. We demonstrated that for higher wave frequencies, collisions are more significant, whereas for lower frequencies, most of the attenuation is due to refraction at the lower boundary of the ionosphere. Changes of attenuation for different wave vector directions can be explained by the classical optical theory of the transmission and reflection of linearly polarized waves in a highly refractive environment with a high Brewster angle. We also compared different models of ionospheric plasma density as well as the amplitude and direction of the intrinsic magnetic field, in order to analyze the influence of these parameters. We showed that decreasing the altitude of the lower ionospheric boundary leads to higher attenuation, with a more significant effect at higher frequencies. An increase in peak ionospheric density with the same shape of profile leads to a rapid increase in the attenuation, which also affects higher frequencies more significantly. The magnitude and inclination of the magnetic field also play a significant role in the wave attenuation. The low magnetic field amplitudes typical for most of the Martian surface cause a high attenuation, primarily affecting higher frequencies. When the magnetic field inclination away from the vertical direction is low, its influence is minimal. However, when the inclination is larger than 50°, the attenuation increases significantly in a nearly horizontal field. These results suggest that the lowest attenuation, and therefore the highest possibility of detecting whistlers, occurs at locations with a strong magnetic field that is nearly vertical.

Acknowledgments. This research was supported by the Ministry of Education, Youth, and Sports under Grant 208 LUAUS23152. KR, IK, and OS were supported by the GACR grant 25-18095X.

References

Akalin, F., Gurnett, D. A., Averkamp, T. F., Persoon, A. M., Santolik, O., Kurth, W. S., and Hospodarsky, G. B., First whistler observed in the magnetosphere of Saturn, *Geophysical Research Letters*, *33*, 2006.

Anderson, M. M., Siemion, A. P. V., Barott, W. C., Bower, G. C., Delory, G. T., de Pater, I., and Werthimer, D., The Allen Telescope Array search for electrostatic discharges on Mars, *The Astrophysical Journal*, *744*, 15, 2011.

Andersson, L., Ergun, R. E., Delory, G. T., Eriksson, A., Westfall, J., Reed, H., McCauly, J., Summers, D., and Meyers, D., The Langmuir Probe and Waves (LPW) Instrument for MAVEN, *Space Science Reviews*, *195*, 173–198, 2015.

Aplin, K. L. and Fischer, G., Lightning detection in planetary atmospheres, *Weather*, *72*, 46–50, 2017.

Aplin, K. L. and Fischer, G., Atmospheric Electricity in the Solar System, in *Oxford Research Encyclopedia of Planetary Science*, Oxford University Press, 2019.

Aplin, K. L., Fischer, G., Nordheim, T. A., Konovalenko, A., Zakharenko, V., and Zarka, P., Atmospheric Electricity at the Ice Giants, *Space Science Reviews*, *216*, 2020.

Barth, E. L., Farrell, W. M., and Rafkin, S. C., Electric field generation in martian dust devils, *Icarus*, *268*, 253–265, 2016.

Gao, J. W., Rong, Z. J., Klinger, L., Li, X. Z., Liu, D., and Wei, Y., A Spherical Harmonic Martian Crustal Magnetic Field Model Combining Data Sets of MAVEN and MGS, *Earth and Space Science*, *8*, e2021EA001 860, e2021EA001860 2021EA001860, 2021.

Graf, K. L., Lehtinen, N. G., Spasojevic, M., Cohen, M. B., Marshall, R. A., and Inan, U. S., Analysis of experimentally validated trans-ionospheric attenuation estimates of VLF signals, *Journal of Geophysical Research: Space Physics*, *118*, 2708–2720, 2013.

Gurnett, D. A., Shaw, R. R., Anderson, R. R., Kurth, W. S., and Scarf, F. L., Whistlers observed by Voyager 1: Detection of lightning on Jupiter, *Geophysical Research Letters*, *6*, 511–514, 1979.

Gurnett, D. A., Kurth, W. S., Cairns, I. H., and Granroth, L. J., Whistlers in Neptune's magnetosphere: Evidence of atmospheric lightning, *Journal of Geophysical Research: Space Physics*, *95*, 20 967–20 976, 1990.

Gurnett, D. A., Morgan, D. D., Granroth, L. J., Cantor, B. A., Farrell, W. M., and Espley, J. R., Non-detection of impulsive radio signals from lightning in Martian dust storms using the radar receiver on the Mars Express spacecraft, *Geophysical Research Letters*, *37*, 2010.

Huba, J. D. and Rowland, H. L., Propagation of electromagnetic waves parallel to the magnetic field in the nightside Venus ionosphere, *Journal of Geophysical Research: Planets*, *98*, 5291–5300, 1993.

Jakosky, B. M., Lin, R. P., Grebowsky, J. M., Luhmann, J. G., Mitchell, D. F., Beutelschies, G., Priser, T., Acuna, M., Andersson, L., Baird, D., Baker, D., Bartlett, R., Benna, M., Bougher, S., Brain, D., Carson, D., Cauffman, S., Chamberlin, P., Chaufray, J.-Y., Cheatom, O., Clarke, J., Connerney, J., Cravens, T., Curtis, D., Delory, G., Demcak, S., DeWolfe, A., Eparvier, F., Ergun, R., Eriksson, A., Espley, J., Fang, X., Folta, D., Fox, J., Gomez-Rosa, C., Habenicht, S., Halekas, J., Holsclaw, G., Houghton, M., Howard, R., Jarosz, M., Jedrich, N., Johnson, M., Kasprzak, W., Kelley, M., King, T., Lankton, M., Larson, D., Leblanc, F., Lefevre, F., Lillis, R., Mahaffy, P., Mazelle, C., McClintock, W., McFadden, J., Mitchell, D. L., Montmessin, F., Morrissey, J., Peterson, W., Possel, W., Sauvaud, J.-A., Schneider, N., Sidney, W., Sparacino, S., Stewart, A. I. F., Tolson, R., Toublanc, D., Waters, C., Woods, T., Yelle, R., and Zurek, R., The Mars Atmosphere and Volatile Evolution (MAVEN) Mission, *Space Science Reviews*, *195*, 3–48, 2015.

Krauss, C. E., Horányi, M., and Robertson, S., Experimental evidence for electrostatic discharging of dust near the surface of Mars, *New Journal of Physics*, *5*, 70, 2003.

Lehtinen, N. G. and Inan, U. S., Radiation of ELF/VLF waves by harmonically varying currents into a stratified ionosphere with application to radiation by a modulated electrojet, *Journal of Geophysical Research: Space Physics*, *113*, 2008.

Lehtinen, N. G. and Inan, U. S., Full-wave modeling of transionospheric propagation of VLF waves, *Geophysical Research Letters*, *36*, 2009.

Melnik, O. and Parrot, M., Propagation of electromagnetic waves through the Martian ionosphere, *Journal of Geophysical Research: Space Physics*, *104*, 12 705–12 714, 1999.

Němec, F., Morgan, D. D., Gurnett, D. A., Duru, F., and Truhlík, V., Dayside ionosphere of Mars: Empirical model based on data from the MARSIS instrument, *Journal of Geophysical Research: Planets*, *116*, 2011.

Peter, K., Pätzold, M., Molina-Cuberos, G. J., González-Galindo, F., Witasse, O., Tellmann, S., Häusler, B., and Bird, M. K., The lower dayside ionosphere of Mars from 14 years of MaRS radio science observations, *Icarus*, *359*, 114 213, 2021.

Ratcliffe, J. A. and Storey, L. R. O., An investigation of whistling atmospherics, *Philosophical Transactions of the Royal Society of London. Series A, Mathematical and Physical Sciences*, *246*, 113–141, 1953.

Riousset, J. A., Nag, A., and Palotai, C., Scaling of conventional breakdown threshold: Impact for predictions of lightning and TLEs on Earth, Venus, and Mars, *Icarus*, *338*, 113 506, 2020.

Ruf, C., Renno, N. O., Kok, J. F., Bandelier, E., Sander, M. J., Gross, S., Skjerve, L., and Cantor, B., Emission of non-thermal microwave radiation by a Martian dust storm, *Geophysical Research Letters*, *36*, 2009.

Scarf, F. L., Gurnett, D. A., Kurth, W. S., Anderson, R. R., and Shaw, R. R., An Upper Bound to the Lightning Flash Rate in Jupiter's Atmosphere, *Science*, *213*, 684–685, 1981.

Stix, T. H., *Waves in plasmas*, Springer Science & Business Media, 1992.